Journal of Magnetic Resonance **145,** 315–318 (2000)
doi:10.1006/jmre.2000.2116, available online at http://www.idealibrary.com on IDEAL®

Imaging of the ^{1}H NMR Second Moment with ^{13}C Chemical-Shift Resolution

M. Nonaka, S. Matsui,[1] and T. Inouye

Institute of Applied Physics, University of Tsukuba, Tsukuba, Ibaraki 305-8573, Japan

Received December 22, 1999; revised May 1, 2000

A method of ^{13}C chemical-shift-resolved ^{1}H second moment imaging is proposed for molecular mobility imaging of heterogeneous materials. For evaluating the ^{1}H second moment, the method relies on the curve fitting procedure using spin-echo shapes indirectly: The information of ^{1}H echo shapes is transferred to the ^{13}C signal amplitude through ^{1}H–^{13}C cross polarization and then the curve fitting is made using the ^{13}C signal amplitude. The ^{13}C signal is detected under ^{1}H dipolar decoupling and magic angle spinning, resulting in the incorporation of ^{13}C chemical-shift resolution. Imaging information is included in the ^{13}C signal by application of phase-encoding gradients. The second moment images obtained can reflect the molecular mobility at every molecular site separated by ^{13}C chemical shifts, yielding detailed information on the molecular mobility. The method is demonstrated by spatially 1D experiments performed on a model sample.

Key Words: **solid-state imaging; second moment; molecular mobility; ^{13}C chemical shift; heteronuclear correlation.**

INTRODUCTION

The utility of NMR imaging for material characterization has been verified by successful applications to solid polymers (*1, 2*). The wealth of image contrast has played an important role in the characterization. Such image contrasts can be obtained from relaxation times and spectroscopic parameters like chemical shifts, providing invaluable information which cannot be obtained with other imaging techniques.

To enhance the utility of NMR imaging even further, novel image contrasts have recently been introduced (*2–4*). One example is the second moment of ^{1}H dipolar spectra (*2, 3*), which can reflect the degree of molecular mobility and is thereby useful for examining the hardness or softness of materials, the crosslink density in elastomers, etc. The method of second moment imaging evaluates the second moment by curve fitting using the peak shape of time-domain spin-echo signals. Since only a few points are usually sufficient for representing the echo peak shape, the method considerably saves the measurement time compared to the method using the frequency-domain spectrum for the evaluation (*2, 3*).

The method of second moment imaging assumes that the second moment value spatially varies depending only on the local molecular mobility. However, this assumption is not necessarily valid for heterogeneous materials. Heterogeneous materials contain many chemically distinctive protons and, as far as proton spin diffusion is negligible, the second moment can be dependent on the chemically distinctive protons as well. For example, the second moment values for methyl and aromatic protons are different when molecular motions are frozen. These chemically distinctive second moments can be separated based on chemical shifts. Each separated second moment can be a measure of the molecular mobility at the corresponding chemically distinctive site, providing much more detailed information about the molecular mobility. Here, we propose a modified method of ^{1}H second moment imaging which enables such separation by making use of ^{13}C isotropic chemical shifts (*5*). The ^{13}C chemical shifts can achieve a far more efficient separation compared to ^{1}H chemical shifts.

METHOD

The pulse sequence for the proposed method of second moment imaging is shown in Fig. 1. This is the spatially 1D version of the ^{13}C chemical-shift-resolved ^{1}H second moment imaging experiment. After preparing the ^{1}H transverse magnetization by a 90° pulse, application of a refocusing pulse or pulse sequence produces a spin echo. This is followed by a spin-locking pulse starting at several points of time in the vicinity of the echo peak ($t_1 = \tau$). In this way, the information of echo peak shape is encoded into the cross-polarization (CP) process and is transferred to the cross-polarized ^{13}C signal amplitude. The second moment is estimated from the transferred information of the echo peak shape by the curve fitting procedure (*2, 3*). The ^{13}C signal is detected under the ^{1}H dipolar decoupling, yielding ^{13}C isotropic chemical shifts. The sample undergoes magic angle spinning (MAS) for averaging out the chemical-shift anisotropies. Prior to ^{13}C detection, the 1D imaging information is included by the phase encoding gradient applied along the MAS axis. (We note that the phase-

[1] To whom correspondence should be addressed. E-mail: matsui@bk.tsukuba.ac.jp.

1090-7807/00 $35.00

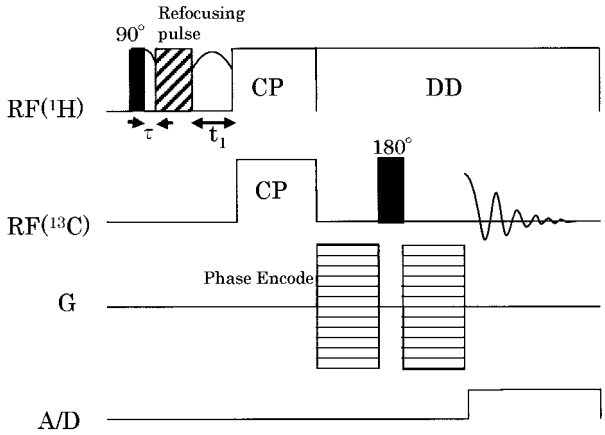

FIG. 1. Pulse sequence for ^{1}H NMR second moment imaging with ^{13}C chemical-shift resolution. The spatially 1D version is shown. The sample undergoes relatively slow magic angle spinning (MAS) and the field gradient (G) is directed along the MAS axis. A spin echo is produced by the application of refocusing pulses. The second moment is extracted by curve fitting from the echo shape, which is encoded into the cross-polarization (CP) process through the incrementation of t_1 (typically, $t_1 = 0 \sim 2\tau$). This produces a ^{13}C magnetization that is amplitude-modulated according to the echo shape. The ^{13}C signal is detected under ^{1}H dipolar decoupling (DD) together with MAS, yielding ^{13}C isotropic chemical shifts.

encoding can be made alternatively to protons just before the spin locking.) For 2D or 3D imaging, multiple gradients must be applied with MAS taken into account (*6*, *7*). The MAS speed must be kept slow such that the second moment is not affected by MAS. TOSS would generally be needed for suppressing spinning sidebands due to the relatively slow MAS.

EXPERIMENTAL

All the experiments were performed on a CMX300 Infinity spectrometer with a CP/MAS imaging probe (*8*). In the preliminary experiments, we used a model sample comprising mixtures of adamantane and hexamethylbenzene powders, which mimics heterogeneous materials. The second moment values for the powders are 0.94 and 2.01 G^2, respectively (*3*). The MAS frequency was set at 800 Hz. The ^{13}C spectrum of the model sample essentially consists of CH and CH_2 peaks from adamantane and a CH_3 peak from hexamethylbenzene, since spinning sidebands from the ring carbons are negligibly weak.

As the spin echo shown in Fig. 1, we chose a solid echo rather than the magic echo which we previously employed (*3*): The magic echo can in principle represent the correct echo shape (*9*), hence the correct second moment. On the other hand, the solid echo shape does not give the correct second moment when the RF pulse spacing is not sufficiently short compared to the transverse relaxation time (*10*). However, the magic echo formation was considerably sensitive to the interference effect by MAS while the solid echo formation was found less sensitive to the MAS interference. For example, when the time interval τ, which is defined by the initial RF pulse spacing in both echoes, was fixed to 30 μs, the second moment obtained from the magic echo started deviating at a MAS frequency of 1.5 kHz. On the other hand, in the case of the solid echo the second moment values remained constant up to a MAS frequency of 3 kHz.

RESULTS AND DISCUSSION

Results of the spatially 1D ^{13}C chemical-shift-resolved ^{1}H second moment imaging experiments performed on the model sample are summarized in Figs. 2, 3, and 4: Fig. 2 shows a representative ^{13}C chemical-shift-resolved spin density image, which was obtained by setting $t_1 = \tau = 30$ μs in the pulse sequence shown in Fig. 1. The 1D adamantane (A) and hexametylbenzene (H) spin density images are separated clearly based on the three ^{13}C chemical shifts, consistent with the chemical composition of the model sample. The theoretical

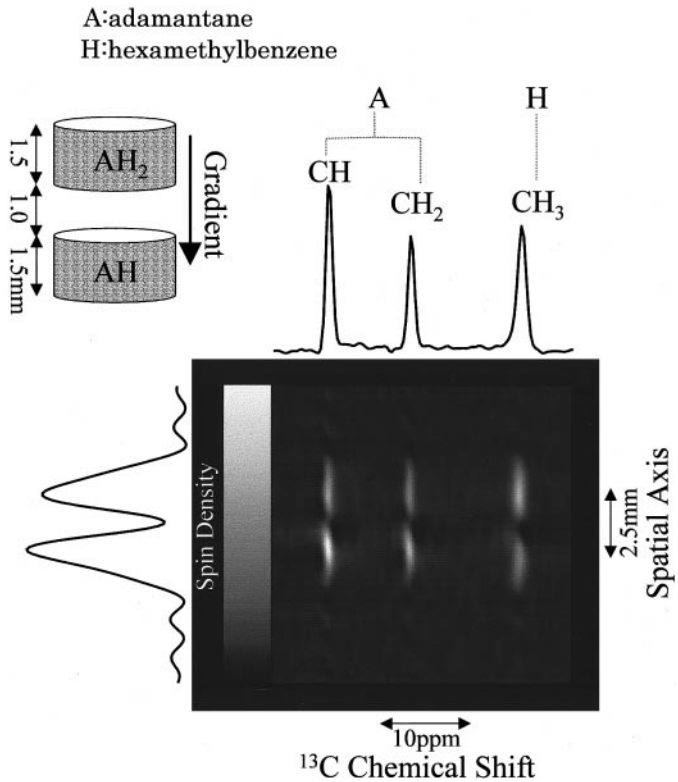

FIG. 2. Representative ^{13}C chemical-shift-resolved spin density image of the model sample shown in this figure. The image is consistent with the chemical composition of the model sample, as indicated by AH and AH_2 (A, adamantane; H, hexamethylbenzene). Effectively 32 phase encodings were made for 2.4 ms with a maximum field gradient of 3 G/cm. The field gradient was directed along the MAS axis. The theoretical spatial resolution is 320 μm and the spectral resolutions are 30, 30, and 80 Hz for CH, CH_2, and CH_3 peaks, respectively. Proton RF field amplitudes were 15 G for 90° pulses and 8 G for CP and DD (Fig. 1). The time intervals for CP and DD were adjusted to 3 and 50 ms. The MAS frequency was 800 Hz. The measurement was repeated 24 times every 5 s.

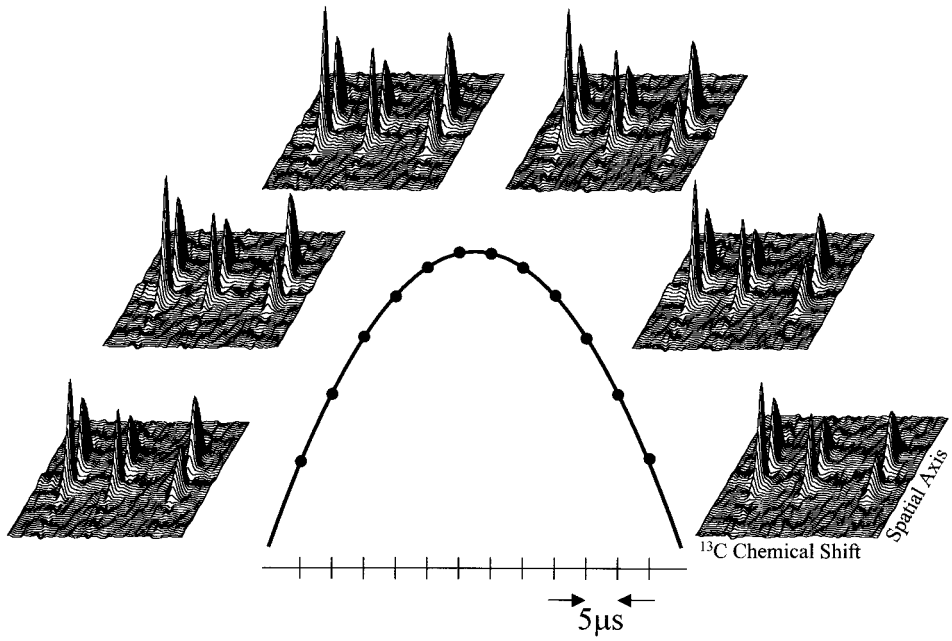

FIG. 3. A series of ^{13}C chemical-shift-resolved spin density images. Only half of the images are shown selected from the total of 12 images. (Unlike the gray-scale image in Fig. 2, 2D plots are used for clarity.) The images were obtained by incrementing the time interval t_1 every 5 μs while τ was fixed at 30 μs (Fig. 1). Note that the image amplitudes are modulated according to the echo peak shapes. Curve fittings using the series of images yield the ^{13}C chemical-shift-resolved ^{1}H second moment image shown in Fig. 4.

spatial resolution is 320 μm and the spectral resolutions are 30, 30, and 80 Hz, for CH, CH_2, and CH_3 peaks, respectively.

Figure 3 displays a series of ^{13}C chemical-shift-resolved 1D spin density images of the model sample. Twelve images were obtained by incrementing the time interval t_1 every 5 μs (Fig. 1) and only half of them are shown. (The number of images, 12, is not necessarily small enough; it was increased intentionally by reducing the accumulation number for each image in order to avoid systematic error due to small instabilities of the spectrometer over the relatively long measurement time, 12.8 h.) Note that the image amplitudes are modulated according to the echo peak shapes. Then, after performing curve fitting at every image pixel, the ^{13}C chemical-shift-resolved ^{1}H second moment image shown in Fig. 4 was obtained. The ^{13}C chemical-shift-resolved ^{1}H second moment image separates and represents faithfully the different values of the second moment, 0.94 G^2 for the CH and CH_2 peaks (adamantane) and 2.01 G^2 for the CH_3 peak (hexamethylbenzene), respectively. The spin diffusion is not negligible between the CH and CH_2 protons in this sample; so the second moment values are the same for the CH and CH_2 peaks.

Our preliminary experimental results have demonstrated the validity of the proposed method of second moment imaging. The proposed variant of the second moment imaging can resolve the sample not only spatially but also chemically, yielding much more detailed information on the molecular mobility in heterogeneous materials such as polymer blends. Although the incorporation of the ^{13}C chemical-shift resolution is associated with undesirable loss in sensitivity due to the ^{13}C signal detection, we believe that there are many situations where such a trade-off made between the sensitivity and the incorporation of the ^{13}C chemical-shift resolution can be justified.

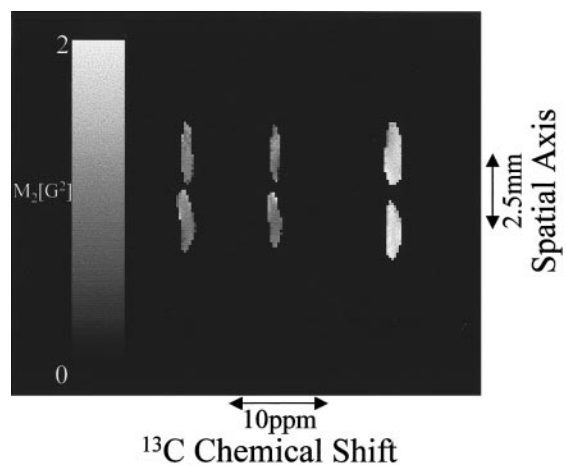

FIG. 4. ^{13}C chemical-shift-resolved ^{1}H second moment image of the model sample shown in Fig. 2. The image was obtained from the series of spin density images shown in Fig. 3 by performing curve fitting at every image pixel. Note that the ^{13}C chemical-shift-resolved ^{1}H second moment image separates and represents faithfully the different values of the second moment, 0.94 G^2 for the CH and CH_2 peaks (adamantane) and 2.01 G^2 for the CH_3 peak (hexamethylbenzene), respectively. The background noise is suitably masked using the image data shown in Fig. 2.

ACKNOWLEDGMENTS

This work was supported by the TARA (Tsukuba Advanced Research Alliance) of the University of Tsukuba and partly by Grant-in-Aid for Science Research 09650061 from the Ministry of Education, Science, and Culture of Japan.

REFERENCES

1. P. Blümler and B. Blümich, "NMR—Basic Principles and Progress," Vol. 30, pp. 209–277, Springer-Verlag, Berlin (1993).
2. F. Weigand, D. E. Demco, B. Blümich, and H. W. Spiess, *Solid State NMR* **6,** 357–365 (1996), and references therein.
3. S. Matsui, M. Nonaka, T. Nakai, and T. Inouye, *Solid State NMR* **10,** 39–44 (1997).
4. T. Nakai, Y. Fukunaga, M. Nonaka, S. Matsui, and T. Inouye, *J. Magn. Reson.* **134,** 44–51 (1998).
5. K. Schmidt-Rohr, J. Clauss, and H. W. Spiess, *Macromolecules* **25,** 3273–3277 (1992).
6. S. Matsui, K. Sekihara, H. Shiono, and H. Kohno, *J. Magn. Reson.* **77,** 182–186 (1988).
7. Y. Sun, H. Lock, T. Shinozaki, and G. E. Maciel, *J. Magn. Reson. A* **115,** 165–173 (1995).
8. S. Matsui, M. Nonaka, T. Nakai, and T. Inouye, *J. Magn. Reson.* **138,** 220–224 (1999).
9. W.-K. Rhim, A. Pines, and J. S. Waugh, *Phys. Rev. B* **3,** 684–695 (1971).
10. J. G. Powells and J. H. Strange, *Proc. Phys. Soc.* **82,** 6–15 (1963).